

ANKRD26 recruits PIDD1 to centriolar distal appendages to activate the PIDDosome following centrosome amplification

Lauren T Evans¹, Taylor Anglen¹, Phillip Scott¹, Kimberly Lukasik^{2,†}, Jadranka Loncarek^{2,†} & Andrew J Holland^{1,*} 

Abstract

Centriole copy number is tightly maintained by the once-per-cycle duplication of these organelles. Centrioles constitute the core of centrosomes, which organize the microtubule cytoskeleton and form the poles of the mitotic spindle. Centrosome amplification is frequently observed in tumors, where it promotes aneuploidy and contributes to invasive phenotypes. In non-transformed cells, centrosome amplification triggers PIDDosome activation as a protective response to inhibit cell proliferation, but how extra centrosomes activate the PIDDosome remains unclear. Using a genome-wide screen, we identify centriole distal appendages as critical for PIDDosome activation in cells with extra centrosomes. The distal appendage protein ANKRD26 is found to interact with and recruit the PIDDosome component PIDD1 to centriole distal appendages, and this interaction is required for PIDDosome activation following centrosome amplification. Furthermore, a recurrent ANKRD26 mutation found in human tumors disrupts PIDD1 localization and PIDDosome activation in cells with extra centrosomes. Our data support a model in which ANKRD26 initiates a centriole-derived signal to limit cell proliferation in response to centrosome amplification.

Keywords ANKRD26; centriole; centriole amplification; PIDDosome

Subject Categories Autophagy & Cell Death; Cell Adhesion, Polarity & Cytoskeleton; Cell Cycle

DOI 10.15252/emboj.2020105106 | Received 25 March 2020 | Revised 8 November 2020 | Accepted 10 November 2020

The EMBO Journal (2020) e105106

Introduction

Centrioles are evolutionarily conserved microtubule-based structures that recruit a surrounding pericentriolar material (PCM) to form the centrosome, an organelle that organizes the interphase microtubule cytoskeleton in many animal cells and forms the poles

of the mitotic spindle (Gonczy, 2012; Nigg & Holland, 2018). Centrioles can also dock at the plasma membrane, where they template the formation of cilia that function in cell signaling, fluid movement, and locomotion. Centriole number is tightly controlled in proliferating cells (Firat-Karalar & Stearns, 2014). G1 cells contain two parent centrioles that differ in age and structure; the younger of the two centrioles was assembled in the previous cell cycle and lacks appendages, while the mature centriole was formed earlier and is decorated with distal appendage structures that are required for membrane docking and ciliogenesis (Nigg & Stearns, 2011; Tanos *et al.*, 2013). At the G1-S transition, one new procentriole grows perpendicularly from a single site at the proximal end of each existing centriole (Tsou & Stearns, 2006). The procentrioles elongate and, in G2, the two centriole pairs separate and increase PCM recruitment to catalyze the formation of the mitotic spindle. Following chromosome segregation, the two centrosomes are divided such that each daughter cell inherits a pair of centrioles.

The faithful control of centriole number is deregulated in a wide range of tumors, leading to either the acquisition of extra copies of centrosomes or centrosome loss (Chan, 2011; Nigg & Holland, 2018; Wang *et al.*, 2019). The presence of supernumerary centrosomes correlates with advanced disease and poor clinical outcome. Centrosome amplification in cultured cells promotes chromosome segregation errors (Ganem *et al.*, 2009; Silkworth *et al.*, 2009) and leads to the accumulation of DNA damage that can drive structural chromosomal alterations (Janssen *et al.*, 2011; Crasta *et al.*, 2012; Ganem & Pellman, 2012). Moreover, extra centrosomes have also been proposed to promote metastasis through multiple distinct mechanisms (Godinho *et al.*, 2014; Arnandis *et al.*, 2018; Ganier *et al.*, 2018a; Ganier *et al.*, 2018b; LoMastro & Holland, 2019). Centrosome amplification has been modeled *in vivo* by increasing the levels of Polo-like kinase 4 (PLK4), the master regulator of centriole duplication. PLK4 overexpression can promote tumorigenesis in both flies and mice (Basto *et al.*, 2008; Coelho *et al.*, 2015; Sercin *et al.*, 2016; Levine *et al.*, 2017). Moreover, the tumors that form in mice with extra centrosomes exhibit complex karyotype changes similar to

1 Department of Molecular Biology and Genetics, Johns Hopkins University School of Medicine, Baltimore, MD, USA

2 Laboratory of Protein Dynamics and Signaling, NIH/NCI/CCR, Frederick, MD, USA

*Corresponding author. Tel: +1 443 287 7433; E-mail: aholland@jhmi.edu

†This article has been contributed to by US Government employees and their work is in the public domain in the USA

those observed in human tumors with centrosome amplification (Levine *et al*, 2017).

Although centrosome amplification is observed across a range of human tumors, extra centrosomes trigger a protective TP53-dependent proliferative block in non-transformed cells in culture (Holland *et al*, 2012; Fava *et al*, 2017). Consistently, dysregulation of the TP53 pathway facilitates the ability of extra centrosomes to promote tumorigenesis in mice (Coelho *et al*, 2015; Sercin *et al*, 2016; Levine *et al*, 2017). Insight into how cells respond to extra centrosomes came from the observation that centrosome amplification triggers activation of a multi-protein complex known as the PIDDosome (Fava *et al*, 2017). The PIDDosome is comprised of caspase-2 (CASP2), PIDD1, and CRADD. PIDD1 and CRADD assemble into a molecular platform that promotes the autocatalytic, proximity-induced activation of CASP2 (Tinel & Tschopp, 2004; Sladky *et al*, 2017). Activated CASP2 then cleaves MDM2, a negative regulator of TP53 stability, resulting in TP53 activation and subsequent upregulation of the cell cycle inhibitor P21 (Oliver *et al*, 2011; Fava *et al*, 2017). This signaling network was shown to limit hepatocyte ploidy in mice (Sladky *et al*, 2020). While activation of the PIDDosome explains how TP53 is stabilized in cells with extra centrosomes, it remains unclear exactly how extra centrosomes activate the PIDDosome and whether inactivation of the PIDDosome increases the long-term fitness of cells with centrosome amplification.

Here we performed a genome-wide CRISPR knockout screen to identify genes required to arrest the proliferation of cells with extra centrosomes. Our results confirm a central role of the PIDDosome in arresting the growth of cells with extra centrosomes. Furthermore, we show that PIDDosome activation requires ANKRD26-dependent recruitment of PIDD1 to the distal appendages of mature parent centrioles. Since cycling cells usually contain only one mature centriole with distal appendages, our data support a model in which extra mature parent centrioles initiate a local signal that activates the PIDDosome in response to centrosome amplification.

Results

A genome-wide CRISPR screen identifies genes required to arrest proliferation following centrosome amplification

To study the impact of centrosome amplification on cell proliferation, we used hTERT immortalized RPE1 cells that can be induced with doxycycline (dox) to overexpress PLK4 (hereafter referred to as PLK4^{Dox}). PLK4^{Dox} cells efficiently cluster extra centrosomes during mitosis and undergo a robust TP53-dependent cell cycle arrest in response to PLK4-induced centrosome amplification (Holland *et al*, 2012). To determine if the cell cycle arrest that occurs following PLK4 overexpression is due to centrosome amplification or an alternative function of PLK4, we created dox-inducible PLK4 cells with or without the centriole protein SAS6. To allow for the continued proliferation of SAS6^{-/-} cells lacking centrioles, we performed experiments in a TRIM37 knockout background (Fong *et al*, 2016; Meitinger *et al*, 2016). While TRIM37-knockout RPE1 cells arrested proliferation after 4 days of PLK4 overexpression, knockout of SAS6 overcame this proliferative arrest (Fig 1A). This suggests the growth arrest induced by PLK4 overexpression is due to centrosome amplification and not PLK4 overexpression *per se*.

To gain insight into how cells respond to extra centrosomes, we designed a genome-wide CRISPR-Cas9 knockout screen to identify genes required to arrest proliferation following centrosome amplification. We utilized PLK4^{Dox} cells carrying a mouse PLK4 transgene that would not be targeted by the human PLK4 sgRNAs encoded in the sgRNA library. We also knocked out USP28 or TRIM37, which allows for cell proliferation following centrosome loss but not following centrosome amplification (Fong *et al*, 2016; Lambrus *et al*, 2016; Meitinger *et al*, 2016). We anticipated two mechanisms by which PLK4-overexpressing, USP28 or TRIM37 knockout cells could be permitted to proliferate: (i) loss of genes required for centriole duplication or stability and (ii) loss of genes required to arrest the growth of cells with extra centrosomes (Fig 1B).

Cas9-expressing PLK4^{Dox}; USP28^{-/-} and PLK4^{Dox}; TRIM37^{-/-} RPE1 cells were infected with a genome-wide sgRNA library containing four independent sgRNAs for every human gene (Fig 1C). Transduced cells were selected for 7 days with puromycin, and knockout libraries of cells were treated with dox to induce centrosome amplification and a subsequent cell cycle arrest. After three weeks of dox treatment, cells were harvested, and sgRNA abundance was analyzed. sgRNAs that provide a growth advantage were expected to enrich in dox treated cells compared with untreated controls. The screen was repeated twice for both PLK4^{Dox}; USP28^{-/-} and PLK4^{Dox}; TRIM37^{-/-} cells, and the data from the four screens were analyzed together using the MAGeCK method for prioritizing genes and pathways (Li *et al*, 2014) (Table EV1; Fig 1D).

Twenty-three of the top 30 hits (FDR ≤ 0.4) identified in our screen were genes that encode proteins reported to localize to the centrosome (Table EV2) (Alves-Cruzeiro *et al*, 2014). From the top 30 hits of our screen, 14 genes had firmly established roles in centriole assembly/stability and were not analyzed further (Fig 1E, Table EV2). We performed competition based-growth assays to validate that knockout of the remaining 16 genes enhanced the proliferation of the PLK4^{Dox}; TRIM37^{-/-} cells used in our screen (Fig EV1A). The only gene that failed to improve the growth of PLK4^{Dox}; TRIM37^{-/-} cells in this assay was *NXT1*, which was excluded from further analysis (Fig EV1B). The remaining 15 genes encoded all of the proteins previously known to be required to arrest the cell cycle in response to centrosome amplification, including all three components of the PIDDosome (*CRADD*, *PIDD1*, and *CASP2*), as well as *TP53* and *P21* (*CDKN1A*) (Fig 1F). We therefore assayed these remaining 15 genes for their role in arresting the growth of cells with extra centrosomes.

We tested the ability of each knockout to enhance the proliferation of PLK4^{Dox} cells using competition growth assays. As expected, sgRNAs targeting *CRADD*, *PIDD1*, *CASP2*, *TP53*, and *P21* increased cell proliferation in response to PLK4 overexpression (Fig 1G). Furthermore, sgRNAs targeting four of the remaining 11 genes tested (*FOPNL*, *C2CD3*, *SCLT1*, and *ANKRD26*) increased the proliferation of cells with centrosome amplification more than three standard deviations above the mean of control cells. Cells expressing sgRNAs targeting each of these genes exhibited high levels of centrosome amplification following PLK4 overexpression, showing that knockout of these genes did not prevent centrosome amplification (Fig 1H). In summary, we identified all the known components of the PIDDosome pathway along with *FOPNL*, *C2CD3*,

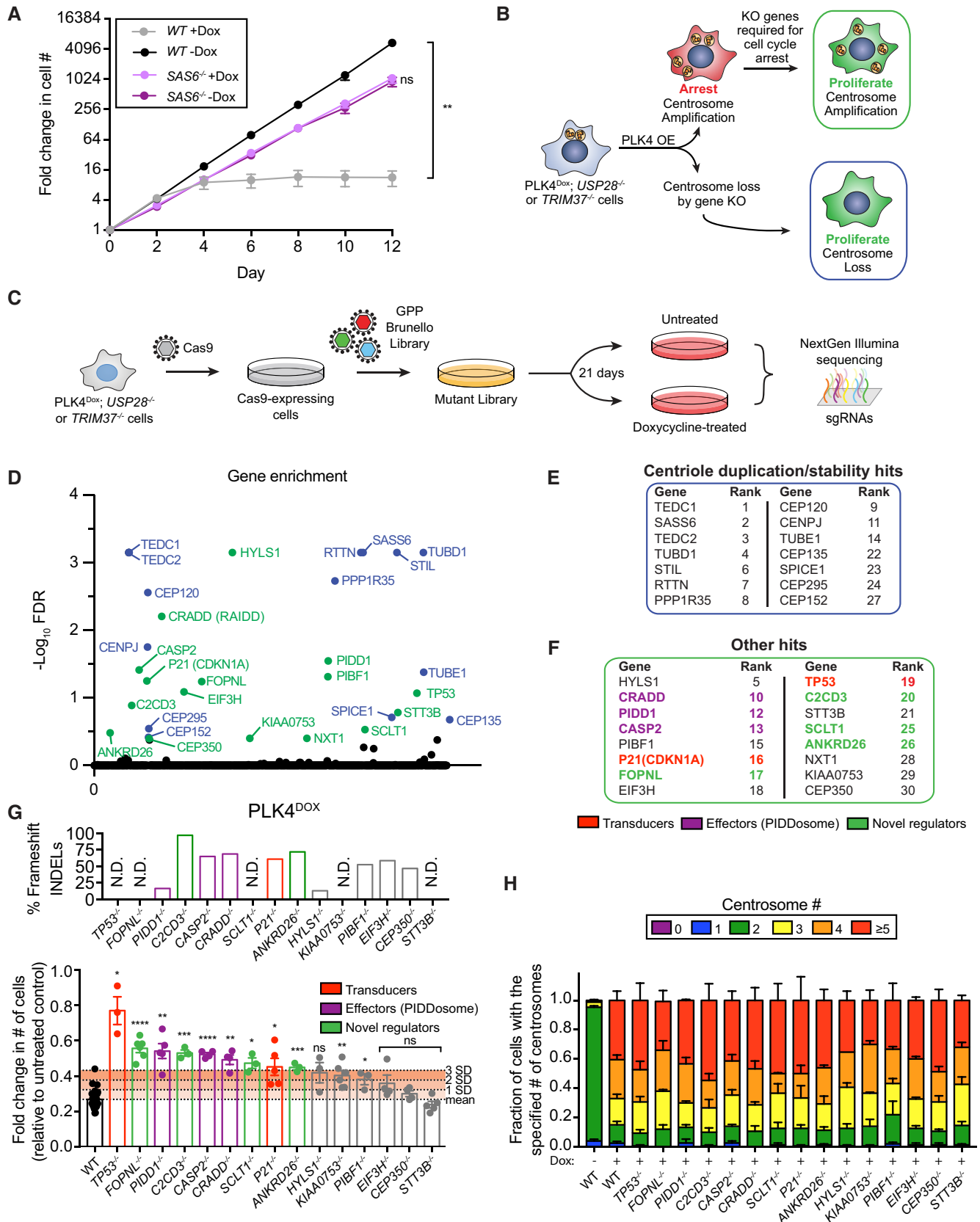


Figure 1.

Figure 1. A CRISPR/Cas9 knockout screen identifies novel genes that arrest the proliferation of cells with centrosome amplification.

- A Growth assay of the indicated cells with and without doxycycline-inducible overexpression of PLK4. Experiments were performed in wild-type or SAS6 monoclonal knockout cells. Data acquired across $n = 3$ biological replicates. Mean \pm s.e.m.
- B Schematic overview of the screen design.
- C Schematic showing the procedure for a CRISPR/Cas9-positive selection screen to identify gene knockouts that increase the proliferation of cells with extra centrosomes.
- D Top hits that emerged from the screens ranked by MaGeCK FDR value. Blue hits are genes required for centriole duplication or stability. Green hits are genes predicted to be required to arrest the growth of cells with extra centrosomes.
- E Hits with a known role in centriole duplication or stability.
- F Candidate hits responsible for arresting the proliferation of cells with centrosome amplification. Purple hits correspond to PIDDosome genes. Red hits correspond to downstream effectors. Green hits are novel regulators.
- G Top: Graph showing the efficiency of frameshifting INDELS measured using TIDE. N.D. = Not determined. Data shown are from $n = 1$ biological replicate. Bottom: Graph showing the relative growth of doxycycline-treated PLK4^{Dox} cells expressing an sgRNA targeting the indicated genes. Each dot displays measurements from a single experiment. Experiments were performed in polyclonal knockout cells. Data acquired across $n \geq 3$ biological replicates. Mean \pm s.e.m.
- H Quantification of centrosome number in PLK4^{Dox} cells expressing an sgRNA targeting the indicated genes. Experiments were performed in polyclonal knockout cells. Data acquired across $n \geq 3$ biological replicates. Mean \pm s.e.m.

Data information: Asterisks indicate statistically significant differences between measurements (* $P < 0.05$; ** $P < 0.01$; *** $P < 0.001$, **** $P < 0.0001$). Statistics for all figures were calculated using a two-tailed Student's t -test. Source data are available online for this figure.

SCLT1, and *ANKRD26* as playing a role in suppressing the proliferation of cells with extra centrosomes.

Centriole distal appendages are required to arrest the cell cycle in response to centrosome amplification

PIDD1 has been reported to decorate mature centrioles (Fava *et al*, 2017). An antibody raised against the PIDD1 death domain showed numerous cytoplasmic foci in addition to a signal that co-localized with the distal appendage of mature parent centrioles (Fig EV1C). The centriole staining of PIDD1 was lost in *PIDD1*^{-/-} RPE1 cells while the cytosolic foci persisted, suggesting that the cytoplasmic staining is likely to be non-specific (Fig EV1D). Consistent with this interpretation, endogenously tagged PIDD1-mNeonGreen localized to the centriole distal appendage in DLD1 cells, but did not label cytosolic structures (Fig EV1E). Importantly, PIDD1 was observed to localize to the distal appendage in both cells with normal and amplified centrosome numbers (Fig EV1C and E). 3D STORM revealed that PIDD1 exhibited a nine-fold localization pattern similar to that of other distal appendage proteins, with an inner and outer diameter of ~ 349 and ~ 595 nm, respectively (Fig 2A–C). PIDD1 localization was most similar to that of *ANKRD26* (Bowler *et al*, 2019), which has previously been shown to localize at the outer portion of the distal appendage and was a hit in our screen.

We tested whether sgRNAs targeting each of the nine genes that function to suppress the growth of cells with extra centrosomes disrupted the centriole recruitment of PIDD1 (Fig 1G). sgRNA-mediated disruption of *CRADD*, *CASP2*, *TP53*, and *P21* did not affect the centriole localization of PIDD1 (Fig 2D). By contrast, sgRNAs targeting the gene *FOPNL*, which encodes a protein required for cilia formation; *C2CD3*, encoding a protein required for distal appendage assembly (Ye *et al*, 2014); or *SCLT1* and *ANKRD26*, which encode distal appendage proteins (Tanos *et al*, 2013; Yang *et al*, 2018; Bowler *et al*, 2019), dramatically reduced the fraction of cells that recruited PIDD1 to the centriole (Fig 2D).

Previous work has established a hierarchy for centriole distal appendage assembly in which *C2CD3* is required to recruit *CEP83*, which recruits *SCLT1* and finally *ANKRD26* (Fig 2E) (Tanos *et al*, 2013; Bowler *et al*, 2019). *C2CD3*, *SCLT1*, and *ANKRD26* were

identified in the top 30 hits of our screens, while *CEP83* did not score highly. To examine the role of all of these genes, we established monoclonal PLK4^{Dox} knockout cell lines for *C2CD3*, *ANKRD26*, *SCLT1*, and *CEP83* (Fig EV1F and G). Knockout of all four genes improved cell proliferation following centrosome amplification (Fig 2F) and almost completely abolished the recruitment of PIDD1 to the mature parent centriole (Figs 2G and EV1H). These data show that distal appendages are required to recruit PIDD1 to mature centrioles and to inhibit cell growth in response to centrosome amplification.

Cells lacking ANKRD26 show improved long-term growth following centrosome amplification

In accord with its localization to the peripheral region of the distal appendage, *ANKRD26* localization at mature centrioles was abolished in *C2CD3*^{-/-}, *SCLT1*^{-/-}, and *CEP83*^{-/-} cells (Figs 3A and EV2A). Moreover, sgRNA-mediated disruption of *FOPNL* also prevented *ANKRD26* and PIDD1 recruitment to the centriole, suggesting that *FOPNL* plays a role in the assembly of the centriole distal appendage (Figs 2G and 3A, and EV1H and EV2A). *ANKRD26*^{-/-} cells had a normal distal appendage localization of *CEP83*, *SCLT1*, *CEP89*, and *CEP164* (Fig 3B and C). Moreover, *ANKRD26*^{-/-} cells formed cilia upon serum starvation at a frequency comparable to wild-type RPE1 cells (Fig 3D and E). These data suggest that the distal appendages remain mostly intact in cells lacking *ANKRD26*.

Knockout of *ANKRD26* allowed the long-term growth of cells with extra centrosomes generated by overexpression of PLK4 (Fig 3F). Importantly, *ANKRD26* was not required for normal centriole duplication, and knockout of *ANKRD26* did not suppress centrosome amplification in cells overexpressing PLK4 (Fig 3G). To test if the extra centrosomes in *ANKRD26*^{-/-} cells could act as microtubule organizing centers (MTOCs), we treated PLK4^{Dox} cells with dox for two days and then added the centrosome declustering agent griseofulvin (Rebacz *et al*, 2007). As expected, extra centrosomes in both wild-type and *ANKRD26*^{-/-} cells nucleated microtubules that led to multi-polar divisions in the presence of griseofulvin (Fig EV2B and C). We conclude that *ANKRD26* is

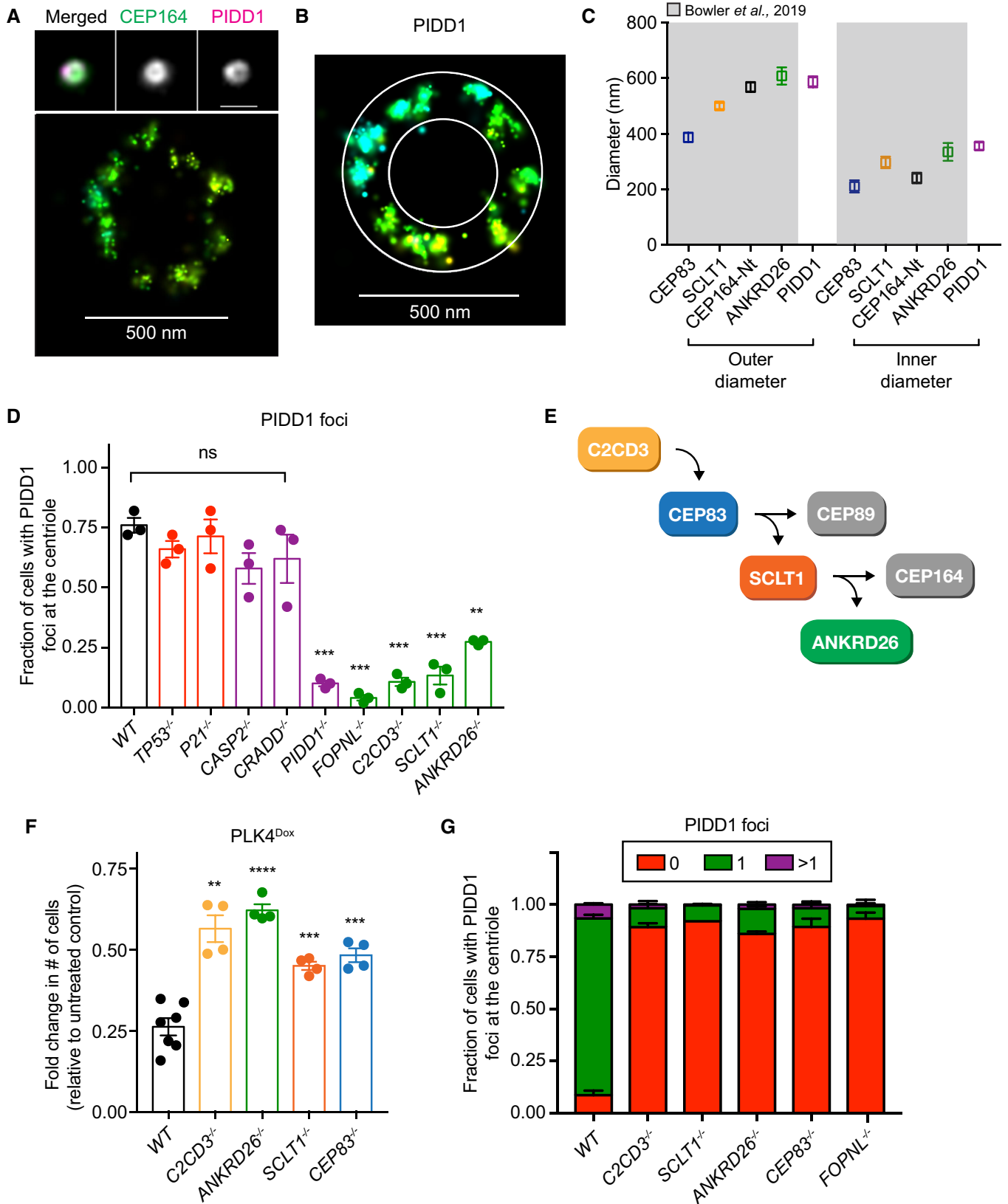


Figure 2.

Figure 2. Distal appendage proteins are required to recruit PIDD1 to the mature parent centriole.

- A Top, wide-field image showing the localization of CEP164 and PIDD1 at the mature mother centriole. Bottom: Representative 3D STORM image of the same centriole showing PIDD1 localization. STORM image colors correspond to the Z-depth with red being the closest to the coverslip and blue being the most distant.
- B 3D STORM image of PIDD1 at the mature mother centriole. The overlaid mask represents the inner and outer diameters of the PIDD1 signal.
- C Inner and outer diameter measurements for distal appendage proteins and PIDD1. Measurements in the shaded region were previously reported in Bowler *et al* (2019). Data displayed as box and whisker plots, where the box represents the upper and lower quartile and the whiskers represent the s.d. Scale bars: 1 μm for all wide-field images of centrioles and 500 nm for STORM images. Data acquired across $n \geq 6$ cells.
- D Quantification of the fraction of cells with PIDD1 localized to the mature mother centriole in PLK4^{Dox} cells expressing an sgRNA targeting the indicated genes. A dot displays measurements from each experiment. Experiments were performed in PLK4^{Dox} polyclonal knockout cells. Data acquired across $n = 3$ biological replicates. Mean \pm s.e.m.
- E Schematic depicting the hierarchy of recruitment of distal appendage proteins.
- F Graph showing the relative growth of doxycycline-treated PLK4^{Dox} cells that were knocked out for the indicated genes. Each dot displays measurements from a single experiment. Experiments were performed in PLK4^{Dox} monoclonal knockout cells. Data acquired across $n \geq 3$ biological replicates. Mean \pm s.e.m.
- G Quantification of the fraction of cells with PIDD1 localized at the mature mother centriole. Experiments were performed in PLK4^{Dox} monoclonal knockout cells. Data acquired across $n = 3$ biological replicates. Mean \pm s.e.m.

Data information: Asterisks indicate statistically significant differences between measurements (** $P < 0.01$; *** $P < 0.001$, **** $P < 0.0001$). Statistics for all Figures were calculated using a two-tailed Student's *t*-test. Source data are available online for this figure.

required to restrict the proliferation of cells following centrosome amplification but is not required for cilia assembly, centriole duplication, or PCM recruitment.

To further test if ANKRD26 suppresses the proliferation of cells with extra centrosomes, we used two additional methods to drive the formation of excessive centrosomes that did not require overexpression of PLK4. First, overexpression of the centriole structural component SAS6 led to centrosome amplification that reduced cell proliferation (Holland *et al*, 2012). This decrease in proliferation was alleviated by knockout of ANKRD26 (Fig EV2D and E). Second, we treated cells with cytochalasin B to induce cytokinesis failure and tested the ability of ANKRD26, PIDD1, and CASP2 to arrest the proliferation of tetraploid cells that have twice the normal centrosome content. Knockout of ANKRD26, PIDD1, or CASP2 increased the fraction of cycling tetraploid cells, indicating that all three of these genes act to restrict the proliferation of newly created tetraploid cells (Fig EV2F and G). We note that the relative increase in growth following loss of ANKRD26 in tetraploid cells was more modest than what was observed in cells with extra centrosomes generated by PLK4 overexpression (Figs 2F and EV2F). This may reflect the shorter duration of the growth assays performed in tetraploid cells (2 days) compared to those carried out in PLK4^{Dox} cells (5 days). Alternatively, tetraploid cells may activate ANKRD26-independent pathways that restrict cell proliferation (Ganem *et al*, 2014).

ANKRD26 links extra centrosomes to PIDDosome activation

To test the effect of ANKRD26 knockout on PIDDosome activation, we monitored the loss of pro-CASP2 and the upregulation of P21 upon centrosome amplification. As expected (Fava *et al*, 2017), the levels of pro-CASP2 decreased, and P21 increased in PLK4^{Dox} cells in a time-dependent manner following dox addition (Fig 3H and I). Knockout of TP53 prevented P21 upregulation but did not affect pro-CASP2 processing following centrosome amplification. By contrast, knockout of ANKRD26 suppressed both CASP2 activation and P21 upregulation in cells with extra centrosomes (Fig 3H and I). These data show ANKRD26 acts as an upstream activator of the PIDDosome and CASP2 in cells with supernumerary centrosomes.

CASP2 is activated in response to several different upstream signals (Sladky & Villunger, 2020). To investigate if the loss of ANKRD26 globally prevents CASP2 activation, we tested the ability of ANKRD26^{-/-} and TP53^{-/-} cells to activate the CASP2 following DNA damage induced by etoposide. While the loss TP53 prevented P21 expression downstream of CASP2 activation, knockout of ANKRD26 did not alter CASP2 activation or P21 induction in cells that experienced DNA damage (Fig EV3A and B). This suggests that ANKRD26 is required to activate CASP2 in cells with extra centrosomes but is not required for CASP2 function *per se*. Notably, CASP2 processing still occurred in PIDD1^{-/-} cells treated with etoposide, suggesting that etoposide-induced CASP2 activation is independent of the PIDDosome (Fig EV3C).

We next investigated if ANKRD26^{-/-} cells were defective in other TP53-dependent response pathways. Knockout of ANKRD26^{-/-} did not affect the ability of cells to arrest following DNA damage, centrosome loss, and chromosome segregation errors (Fig EV3D). Moreover, ANKRD26^{-/-} cells also underwent H₂O₂-induced arrest at similar levels to control cells (Fig EV3D). By contrast, TP53^{-/-} cells exhibited enhanced growth in all of these conditions. Since upstream components of the DNA damage and senescence pathways did not emerge as hits in our screen, we conclude that ANKRD26-mediated activation of TP53 is functionally distinct from the DNA damage and senescence response pathways.

The ANKRD26 coiled-coil region binds to the UPA domain of PIDD1

To determine which region of ANKRD26 is required to recruit PIDD1 to the distal appendage, we expressed deletion mutants of mCherry-ANKRD26 in ANKRD26^{-/-} cells and monitored PIDD1 recruitment to the centriole. The deletion of the ANKRD26 N-terminus (amino acids 1–344) led to a partial reduction in the centriole recruitment of ANKRD26 and PIDD1 (Fig EV4A–D). In contrast, deletion of the ANKRD26 C-terminus (amino acids 1,231–1,710) prevented the centriole localization of both proteins (Fig EV4A–D). This suggests that the N and C-terminal region of ANKRD26 both play a role in recruitment to the centriole.

The deletion of the ANKRD26 M1 region (amino acids 345–849) had no impact on the centriole recruitment of ANKRD26, but partly

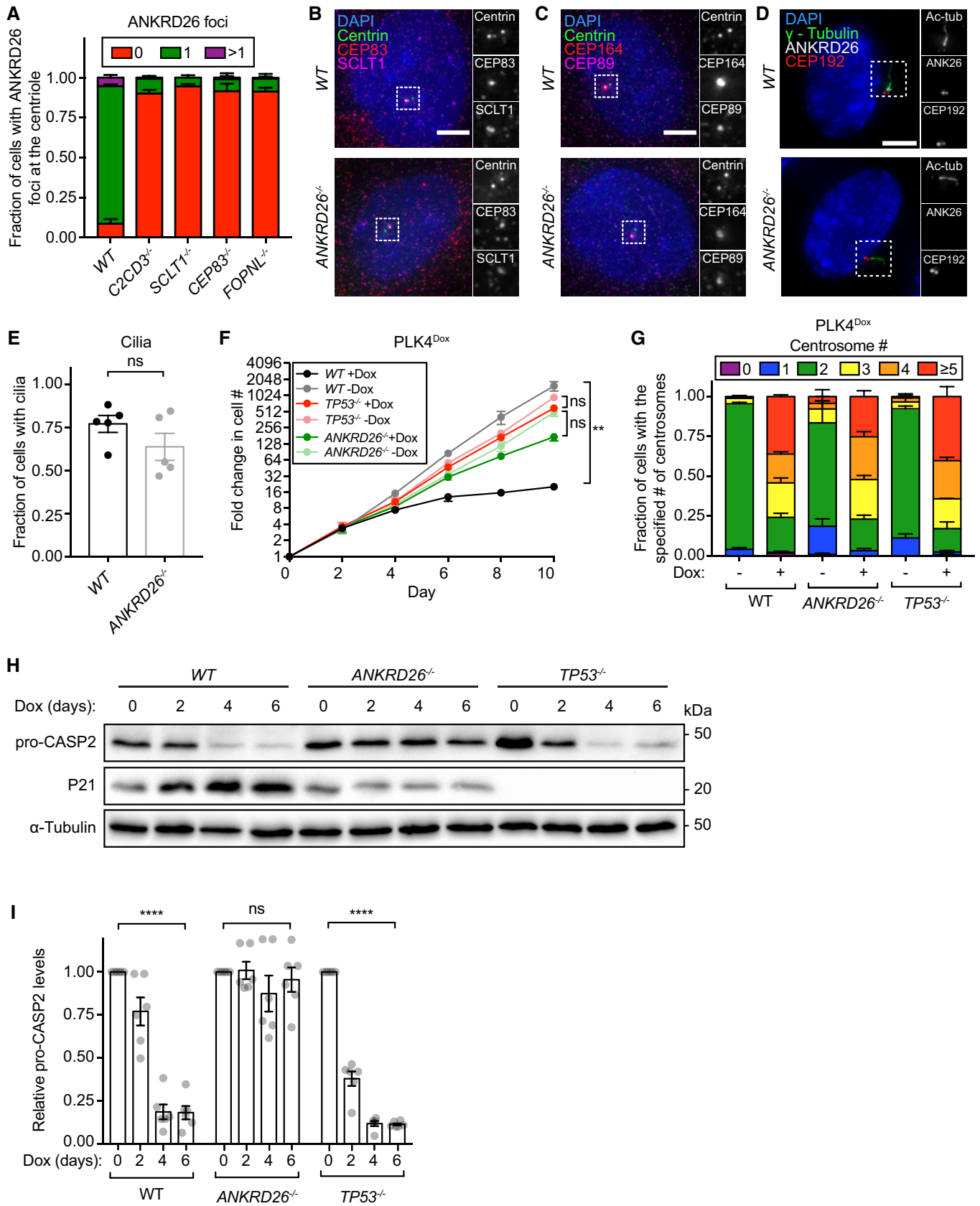


Figure 3.

Figure 3. ANKRD26 is required to arrest cell proliferation in response to centrosome amplification.

- A Quantification of the fraction of cells with ANKRD26 localized at the mature mother centriole. Experiments were performed in PLK4^{Dox} monoclonal knockout cells. Data acquired across $n = 3$ biological replicates. Mean \pm s.e.m.
- B–D Representative images of *WT* or *ANKRD26*^{-/-} cells immunostained with the indicated antibodies. Scale bar = 5 μ m.
- E Quantification of the fraction of *WT* or *ANKRD26*^{-/-} hTERT RPE1 cells with cilia. Each dot displays measurements from a single experiment. Data acquired across $n = 5$ biological replicates. Mean \pm s.e.m.
- F Growth assay of the indicated cells with and without doxycycline-inducible overexpression of PLK4. Experiments were performed in PLK4^{Dox} monoclonal knockout cells. Data acquired across $n = 3$ biological replicates. Mean \pm s.e.m.
- G Quantification of centrosome number in PLK4^{Dox} cells expressing an sgRNA targeting the indicated genes. Experiments were performed in PLK4^{Dox} monoclonal knockout cells. Data acquired across $n = 3$ biological replicates. Mean \pm s.e.m.
- H Western blot showing expression of pro-CASP2 and P21 following treatment with dox for the specified number of days. Experiments were performed in PLK4^{Dox} monoclonal knockout cells.
- I Quantification of pro-CASP2 levels following treatment with dox for the specified number of days. Experiments were performed in PLK4^{Dox} monoclonal knockout cells. Each dot displays measurements from a single experiment. Data acquired across $n = 6$ biological replicates. Mean \pm s.e.m.

Data information: Asterisks indicate statistically significant differences between measurements (** $P < 0.01$; **** $P < 0.0001$). Statistics for all Figures were calculated using a two-tailed Student's *t*-test.

Source data are available online for this figure.

compromised the centriole localization of PIDD1. Notably, an ANKRD26^{AM2} mutant lacking amino acids 850–1,320 localized to the centriole, but completely failed in the recruitment of PIDD1 (Fig EV4A–D). These data indicate that the 850–1,320 amino acid region of ANKRD26 is required for the recruitment of PIDD1 to the centriole distal appendage.

The 850–1,320 amino acid region of ANKRD26 contains a conserved coiled-coil region (amino acids 913–1,216) (Fig EV4A). To establish if this coiled-coil region is responsible for binding to PIDD1, we overexpressed in cells with a normal centrosome content mCherry-ANKRD26 coiled-coil (mCherry-ANKRD26^{CC}) and wild-type PIDD1-FLAG. Purified mCherry-ANKRD26^{CC} associated with PIDD1-FLAG, showing that the coiled-coil region of ANKRD26 is sufficient for PIDD1 binding (Fig 4A).

Full-length PIDD1 is processed into three fragments: an N-terminal piece called PIDD1-N and two C-terminal fragments, PIDD1-C and PIDD1-CC, respectively (Fig 4A). Cleavage occurs at S446 and S588 through an autoproteolytic process similar to the mechanism described by self-cleaving protein segments such as inteins (Tinel *et al*, 2007). Full-length PIDD1 is rapidly processed in cells to form PIDD1-C, while the second cleavage event that forms the PIDD1-CC fragment is stimulated by specific inputs (Sladky *et al*, 2017, 2020). To define the region of PIDD1 that interacts with ANKRD26, we expressed in cells mCherry-ANKRD26^{CC} along with FLAG-tagged PIDD1-N, PIDD1-C, and PIDD1-CC. mCherry-ANKRD26^{CC} interacted with the PIDD1-C and PIDD1-CC fragments but failed to bind PIDD1-N (Fig 4A). Importantly, ANKRD26^{CC} did not bind to PIDD1 lacking the CC fragment (PIDD1^{ΔCC}), demonstrating that the CC fragment of PIDD1 is both necessary and sufficient for ANKRD26 binding (Fig 4B).

The PIDD1-CC region contains a UPA domain of unknown function (Wang *et al*, 2009) and a death domain (DD) that binds to CRADD to form the PIDDosome (Park *et al*, 2007). To establish which of these domains are responsible for associating with ANKRD26, we tested the ability of PIDD1 mutants lacking the UPA domain or DD to bind to ANKRD26^{CC}. ANKRD26^{CC} robustly interacted with PIDD1 lacking the DD (PIDD1^{ΔDD}), but only weakly associated with PIDD1 deleted of the UPA domain (PIDD1^{ΔUPA}) (Fig 4B). This suggests that the coiled-coil region of ANKRD26 predominantly associates with the PIDD1 UPA domain.

A non-cleavable mutant of PIDD1 retained its ability to interact with ANKRD26^{CC}, arguing that PIDD1 cleavage is not required to

bind to ANKRD26 (Fig 4B). In fact, ANKRD26^{CC} preferentially binds to unprocessed, full-length PIDD1 (Fig 4B). Since the PIDD1-N and PIDD1-C cleavage fragments remain associated in a complex after processing (Tinel *et al*, 2007), this raised the possibility that ANKRD26 associates with the UPA domain of unprocessed PIDD1 and that following cleavage, PIDD1-N inhibits the binding of ANKRD26^{CC} to PIDD1-C. To test this hypothesis, we co-expressed PIDD1-N-MycGFP, mCherry-ANKRD26^{CC}, and PIDD1-C-FLAG, and immunoprecipitated mCherry-ANKRD26^{CC} or PIDD1-N-MycGFP (Fig EV4E and F). As expected, PIDD1-N-MycGFP interacted with PIDD1-C-FLAG (Tinel *et al*, 2007). Notably, however, the interaction of PIDD1-C with ANKRD26^{CC} decreased when PIDD1-N was expressed. Therefore, PIDD1-C preferentially associates with PIDD1-N and this binding inhibits the association of PIDD1-C with ANKRD26.

The C-terminal fragment of PIDD1 is required for its centriole localization

To determine which region of PIDD1 is responsible for its recruitment to the centriole, we generated *PIDD1*^{-/-} RPE1 cells stably expressing mCherry-PIDD1-N or untagged full-length PIDD1, non-cleavable PIDD1, PIDD1-C, or PIDD1-CC. We evaluated the localization of full-length PIDD1, non-cleavable PIDD1, PIDD1-C, and PIDD1-CC using an antibody raised against the PIDD1 death domain. The PIDD1-N fragment lacked the death domain and was visualized using the mCherry tag. As expected, both full-length and non-cleavable PIDD1 localized to the mature parent centriole (Fig EV4G and H). The PIDD1-C and PIDD1-CC fragments that are capable of binding to ANKRD26 were also recruited to the centriole, but at a significantly diminished level compared with full-length PIDD1. By contrast, the PIDD1-N fragment that failed to interact with ANKRD26 showed no centriole localization (Fig EV4G and H). These data suggest that the PIDD1-CC fragment is responsible for binding to ANKRD26 and recruiting PIDD1 to the centriole.

ANKRD26-mediated recruitment of PIDD1 to the distal appendage is required for PIDDosome activation

To test the role of ANKRD26-mediated recruitment of PIDD1 in activating the PIDDosome, we expressed a mCherry-ANKRD26 or

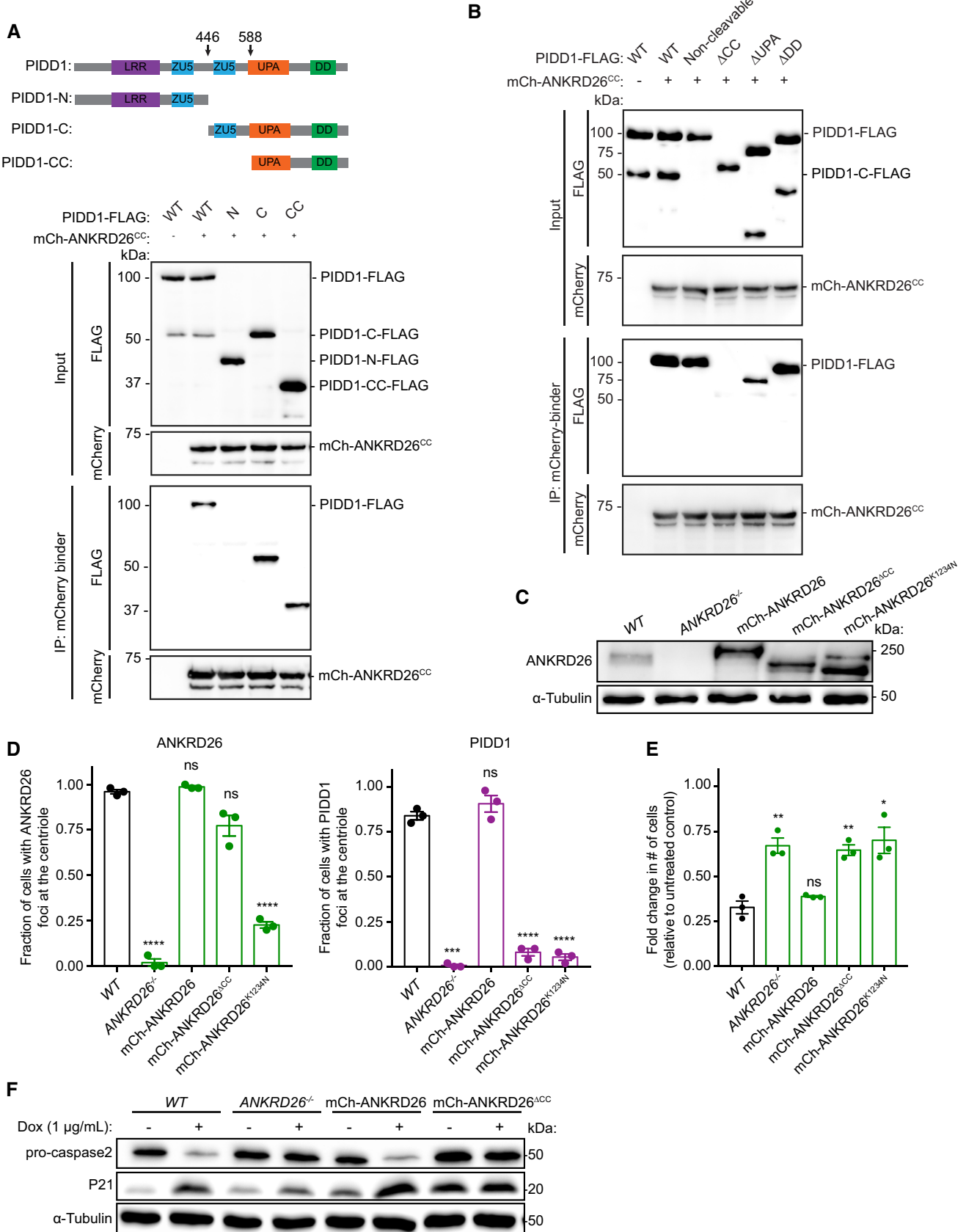


Figure 4.

Figure 4. The coiled-coil domain of ANKRD26 is required for PIDD1 recruitment to the centriole and PIDDosome activation following centrosome amplification.

- A Top: schematic representation of PIDD1 and its cleavage products. Bottom: HEK293FT cells were transfected with the indicated constructs, subjected to co-immunoprecipitation and immunoblotted with the indicated antibodies.
- B HEK293FT cells were transfected with the indicated constructs, subjected to co-immunoprecipitation and immunoblotted with the indicated antibodies.
- C Western blot showing the expression of ANKRD26. Experiments were performed in monoclonal ANKRD26^{-/-} PLK4^{Dox} cells expressing the indicated ANKRD26 transgenes.
- D Quantification of the fraction of cells with ANKRD26 (left) and PIDD1 (right) localized to the mature mother centriole in monoclonal ANKRD26^{-/-} PLK4^{Dox} cells expressing the indicated transgenes. Each dot displays measurements from a single experiment. Data acquired across $n = 3$ biological replicates. Mean \pm s.e.m.
- E Graph showing the relative growth of doxycycline-treated, monoclonal ANKRD26^{-/-} PLK4^{Dox} cells expressing the indicated ANKRD26 transgenes. Each dot displays measurements from a single experiment. Data acquired across $n = 3$ biological replicates. Mean \pm s.e.m.
- F Western blot showing expression of pro-CASP2 and P21 following treatment with dox for 4 days. Experiments were performed in monoclonal ANKRD26^{-/-} PLK4^{Dox} cells expressing the indicated transgenes.

Data information: Asterisks indicate statistically significant differences between measurements (* $P < 0.05$; ** $P < 0.01$; *** $P < 0.001$, **** $P < 0.0001$). Statistics for all Figures were calculated using a two-tailed Student's t -test.

Source data are available online for this figure.

mCherry-ANKRD26^{ACC} transgene in ANKRD26^{-/-} PLK4^{Dox} cells (Fig 4C). Expression of a wild-type mCherry-ANKRD26 transgene rescued PIDD1 recruitment to the mature parent centrioles (Fig 4D). Furthermore, wild-type mCherry-ANKRD26 promoted PIDDosome activation and suppressed the proliferation of cells with extra centrosomes (Fig 4E and F). By contrast, although the mCherry-ANKRD26^{ACC} mutant localized to the centriole, it could not recruit PIDD1 to the distal appendage (Fig 4D). Importantly, the mCherry-ANKRD26^{ACC} mutant did not restrict proliferation in cells with extra centrosomes nor did it induce PIDDosome activation (Fig 4E and F). This suggests that ANKRD26-mediated recruitment of PIDD1 to the distal appendage is required for PIDDosome activation and growth arrest following centrosome amplification.

A recurrent cancer mutation disrupts the ability of ANKRD26 to arrest the proliferation of cells with extra centrosomes

We investigated whether defects in ANKRD26-mediated PIDDosome activation occur in human cancers. Interestingly, a single nucleotide deletion in ANKRD26 was found in 20 independent tumors from the colon, stomach, uterus, and brain (Fig EV5A) (Cerami *et al*, 2012). This one base pair deletion resulted in a K1234N mutation and a premature translational stop that truncated ANKRD26 just after the CC domain that interacts with PIDD1 (Fig EV4A). The striking recurrence of the same mutation suggests that the K1234Nfs*19 alteration is selected for in these cancers. To test the impact of this mutation on ANKRD26-mediated PIDDosome activation, we expressed a mCherry-ANKRD26 K1234Nfs*19 transgene in ANKRD26^{-/-} PLK4^{Dox} cells (Fig 4C).

Similar to what was observed following the deletion of the ANKRD26 C-terminus (amino acids 1,231–1,710) (Fig EV4A–D), the mCherry-ANKRD26 K1234Nfs*19 mutant localized inefficiently to the centriole and was defective in recruiting PIDD1 to the distal appendage (Fig 4D). This mutant also failed to promote PIDDosome activation or restrict the proliferation of cells with extra centrosomes. This suggests that the K1234Nfs*19 mutation disrupts the ability of ANKRD26 to localize to the centriole and trigger PIDD1 activation following centrosome amplification (Fig 4E and F).

TP53 functions downstream of ANKRD26 to arrest the growth of cells with extra centrosomes. Given that TP53 loss of function frequently occurs in human tumors and would be expected to overcome the requirement for ANKRD26-disrupting mutations, we

analyzed the fraction of ANKRD26 K1234Nfs*19 tumors that also showed oncogenic TP53 alterations. Of the 20 tumors containing K1234N mutations, 15% also contained an oncogenic TP53 alteration, and an additional 15% have a TP53 variant of unknown significance (Table EV3). This fraction is lower than the overall frequency of TP53 alterations observed for each tumor type subtype. However, since the number of tumors analyzed is small, no definitive conclusions can be drawn at this stage.

Discussion

Centrosome amplification has been shown to activate the PIDDosome and stabilize TP53 to limit cell proliferation (Holland *et al*, 2012; Fava *et al*, 2017). However, the mechanism by which excessive numbers of centrosomes activate the PIDDosome remained unclear. Using an unbiased, genome-wide screen, we discovered five new proteins that restrict the proliferation of cells with extra centrosomes. All of these proteins localize to or are required for the assembly of centriole distal appendages. Moreover, we show that one of these proteins, the distal appendage protein ANKRD26, binds to and recruits PIDD1 to the centriole. This binding interaction is required for PIDDosome activation in response to centrosome amplification. We found that ANKRD26 preferentially interacts with the UPA domain of unprocessed PIDD1. Our data suggest that following auto-cleavage, the PIDD1-N fragment outcompetes the binding of ANKRD26 to the PIDD1 UPA domain. This would result in processed PIDD1 being released from binding to ANKRD26 at the distal appendage. Notably, the other PIDDosome components (CRADD and CASP2) do not appear to localize to the centriole but are needed to arrest the cell cycle in response to centrosome amplification. This suggests a model in which ANKRD26 “primes” PIDD1 at the distal appendage and releases processed PIDD1 into the cytoplasm, where it interacts with CRADD to promote CASP2 processing (Fig 5).

The requirement of centriole distal appendages for PIDDosome activation following centrosome amplification suggests that these structures are being actively monitored in cells. This is consistent with a previous model where an increase in the number of mature parent centrioles was shown to be the cue that triggers PIDDosome activation (Fava *et al*, 2017). PIDD1 decorates the appendages of all mature parent centrioles irrespective of their number, raising the

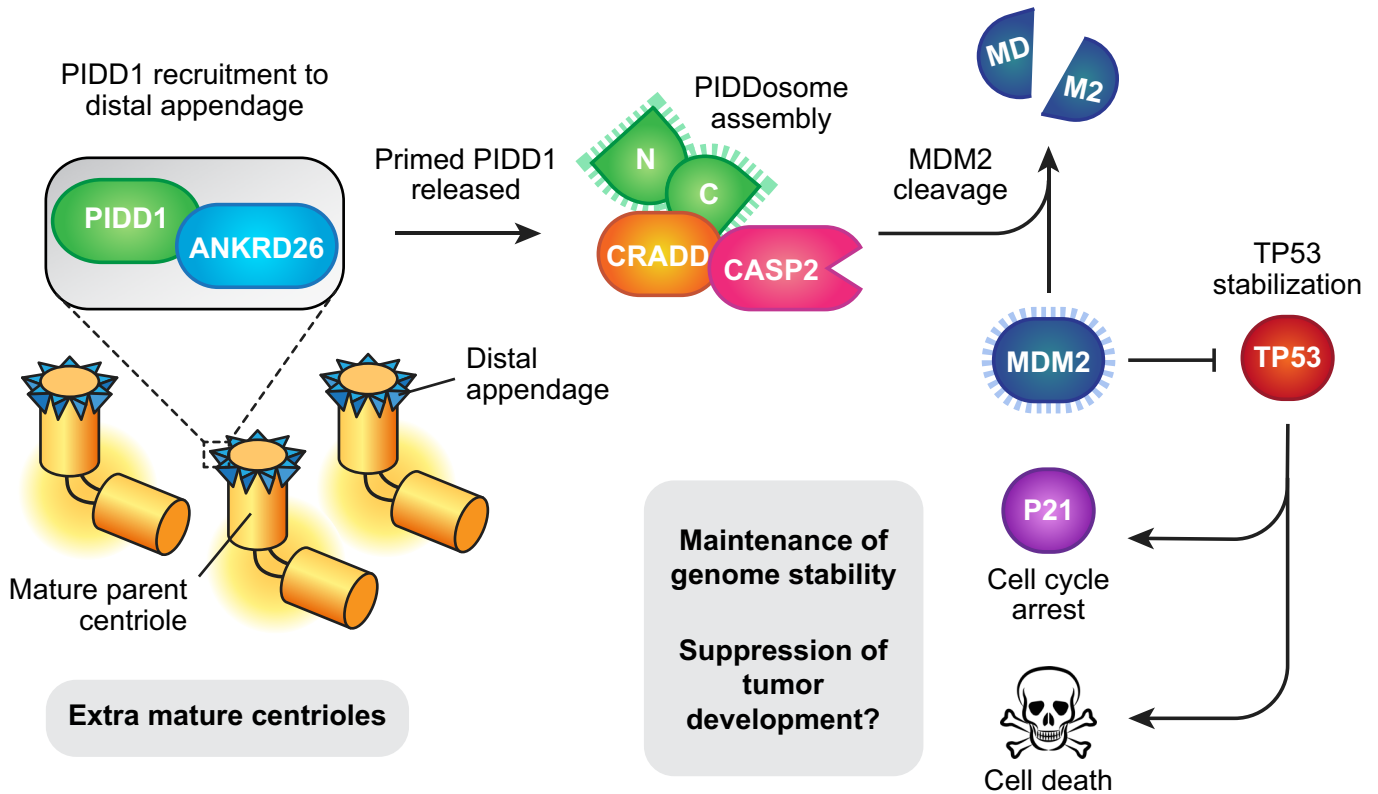


Figure 5. A model for PIDDosome activation in cells with extra centrosomes.

Cycling cells normally contain a single mature parent centriole that is decorated with distal appendages. PIDD1 is recruited by ANKRD26 to the centriole distal appendage. In the presence of extra mature parent centrioles, PIDD1 is activated at the distal appendage and released into the cytoplasm to promote PIDDosome assembly and caspase-2 activation. Active caspase-2 cleaves MDM2 leading to stabilization of P53 and subsequent cell cycle arrest or cell death.

question of how PIDD1 monitors the presence of excessive numbers of mature centrioles. One possibility is that extra mature centrioles dilute out one or more components of the distal appendage, leading to structural aberrations that induce a conformational change in PIDD1 to allow for PIDDosome assembly. In this regard, it will be interesting to examine the distal appendage structure by super-resolution and electron microscopy in cells with normal and extra mature parent centrioles. An alternative possibility is that the clustering of multiple mature parent centrioles after mitosis brings about a conformational change in PIDD1 at the distal appendage that leads to PIDDosome assembly (Fava *et al.*, 2017). Indeed, in interphase cells, supernumerary mature centrioles are often orientated with their distal appendages ~ 600 nm apart (Fig EV5B). Moreover, we observed a ~ 30% decrease in the average distance between the distal appendages of the closest parent centrioles in arrested cells compared with cycling cells, but this difference did not reach statistical significance (Fig EV5B–D). In the future, it will be important to determine if centriole clustering in interphase is required to trigger PIDDosome activation in cells with extra centrosomes. Finally, it is plausible that a mature parent centriole produces a low-level of active PIDD1 that is below the threshold level required for PIDDosome assembly. The presence of extra mature centrioles may push the amount of active PIDD1 above the threshold needed to trigger a cell cycle arrest. Identifying the turnover kinetics of endogenous

PIDD1 at the centriole distal appendage will be critical to test this model.

Loss of ANKRD26 enables the continued proliferation of cells with extra centrosomes, raising the question of whether inactivation of this pathway is selected for during tumorigenesis. Loss of ANKRD26 would be predicted to offer no fitness advantage in tumor cells that lack TP53 functionality, perhaps explaining why ANKRD26 mutations are not commonly observed in human cancers. Nevertheless, we identified a recurrent frameshift mutation in ANKRD26 (K1234Nfs*19) observed in multiple stomach, brain, uterine, and colon tumors. This mutation leads to the expression of a truncated form of ANKRD26 that fails to recruit PIDD1 to the centriole and activate the PIDDosome in response to centrosome amplification. This suggests that loss of ANKRD26-mediated PIDD1 signaling is selected for in some human tumors. It is plausible that the K1234Nfs*19 ANKRD26 mutation enables the continued propagation of tumor cells with extra centrosomes, and it will be interesting to examine if selection for this mutation co-occurs with centrosome amplification in cancer cells.

In addition to a possible role of ANKRD26 mutations in tumorigenesis, mutations in the 5'UTR of the ANKRD26 gene cause an autosomal-dominant form of thrombocytopenia due to reduced blood platelet production by megakaryocytes (Pippucci *et al.*, 2011; Noris *et al.*, 2013). During their maturation, megakaryocytes undergo

several rounds of endomitosis to produce large polyploid cells with extra centrosomes (Moskvina-Tarkhanov & Onishchenko, 1978; Vitrat *et al*, 1998; Falcieri *et al*, 2000). Thrombocytopenia-associated mutations in *ANKRD26* lead to the persistent expression of *ANKRD26* during the late stages of megakaryocyte development, and, consequently, megakaryocytes from these patients exhibit reductions in cell ploidy (Bluteau *et al*, 2014). Based on our observations, it is tempting to speculate that the reduction in megakaryocyte ploidy in these patients arises due to *ANKRD26*-mediated activation of the PIDDosome in megakaryocytes with extra centrosomes (Bluteau *et al*, 2014). Patients with mutations in the 5'UTR of *ANKRD26* also exhibit an increased incidence of myeloid malignancies (Pippucci *et al*, 2011; Noris *et al*, 2013; Marquez *et al*, 2014), and N-terminal truncating mutations in *ANKRD26* have been identified in sporadic, adult-onset AML cases (Marconi *et al*, 2017). How these *ANKRD26* mutations lead to an increased incidence of hematological malignancies remains unclear.

Many human tumors arise from a tetraploid intermediate containing twice the normal DNA and centrosome content (Zack *et al*, 2013; Bielski *et al*, 2018). At least two pathways appear to have evolved to restrict the proliferation of genomically unstable tetraploid cells. First, extra centrosomes in tetraploid cells activate the PIDDosome and CASP2 to inactivate MDM2 (Oliver *et al*, 2011; Fava *et al*, 2017; Sladky *et al*, 2020). Second, tetraploid cells hyper-activate Rac1, which leads to a decline in RhoA-GTP (Godinho *et al*, 2014). Decreased RhoA-GTP leads to activation of the hippo pathway kinase LATS2, which stabilizes p53 through inhibition of MDM2 (Ganem *et al*, 2014). Correspondingly, RNAi knockdown of LATS2 enables tetraploid cells to overcome a G1 cell cycle arrest (Ganem *et al*, 2014). However, it is notable that we did not identify LATS2 in our screen for genes that limit the proliferation of cells with extra centrosomes. We envisage several possible explanations for this discrepancy. First, there may be differences in the fitness of LATS2 knockout cells generated using CRISPR/Cas9 in our study and cells depleted of LATS2 by RNAi in the Ganem *et al*, study. Second, knockdown of LATS2 was shown to enable tetraploid cells to progress into S phase, but may not offer the long-term growth advantage that would be required to score as a hit in our screen. Third, activation of LATS2 in tetraploid cells may not only be driven by an increased number of centrosomes and could rely on other features of tetraploid cells, such as the increased DNA content or reduced surface area to volume ratio (Ganem *et al*, 2014). Finally, tetraploid cells are expected to contain two mature parent centrioles. A more dramatic increase in parent centriole number following PLK4 overexpression could lead to more robust PIDDosome activation and a greater reliance on this pathway to suppress proliferation.

In conclusion, we have identified a new role for the centriole distal appendage protein *ANKRD26* in signaling to the PIDDosome. Mammalian centrosomes have long been proposed to function as signaling hubs in a manner analogous to the related spindle pole bodies (SPB) of yeast (Arquint *et al*, 2014). However, while yeast SPBs have established roles in controlling entry into and exit from mitosis (Hagan & Grallert, 2013; Fu *et al*, 2015), there is a lack of definitive evidence for a role of vertebrate centrosomes in cell signaling. Our finding that distal appendages of mature parent centrioles deliver a signal required to activate the PIDDosome offers new support for a role of centrosomes in controlling cell proliferation in human cells.

Materials and Methods

Cell culture and drug treatments

RPE-1 cells were grown in DMEM:F12 50:50 medium (Cellgro; Corning) containing 10% fetal bovine essence (Seradigm), 0.348% sodium bicarbonate, 100 U/ml penicillin, 100 U/ml streptomycin, and 2 mM L-glutamine. HEK293FT and DLD1 cells were grown in DMEM medium (Cellgro; Corning) containing 10% fetal bovine essence (Seradigm), 100 U/ml penicillin, 100 U/ml streptomycin, and 2 mM L-glutamine. RPE-1 and DLD1 cells were validated by STR genotyping. Cells were maintained at 37°C in a 5% CO₂ atmosphere with 21% oxygen. Doxycycline (Millipore Sigma) was diluted in water and used at a final concentration of 1 µg/ml. Etoposide (Millipore Sigma) was diluted in DMSO and used at a final concentration of 50 µM. Doxorubicin (Sigma-Aldrich) was diluted in DMSO and used at a final concentration of 50 ng/µl. Reversine (Sigma-Aldrich) was diluted in DMSO and used at a final concentration of 500 nM. Centrinone (Tocris) was dissolved in DMSO and used at a final concentration of 125 nM. Griseofulvin (Sigma-Aldrich) was diluted in DMSO and used at a final concentration of 25 µM. Hydrogen peroxide 30% w/w (Sigma-Aldrich) was diluted in water and used at a final concentration of 150 nM. All cell lines were determined to be free from mycoplasma contamination using DAPI staining.

Lentiviral production and transduction

The pLentiGuide-puromycin (117986; Addgene), pLentiCRISPR-v2-Neomycin (127644; Addgene), Lenti-CMV-Zeocin (this study), Tet-ON mPLK4 or Tet-ON hSAS6 lentiviral plasmid was co-transfected into HEK293FT cells with the lentiviral packaging plasmids psPAX2 and pMD2.G (12260 and 12259; Addgene). In brief, 3×10^6 HEK293FT cells were seeded into a poly-L-Lysine-coated 10 cm culture dish the day before transfection. For each 10 cm dish, the following DNA was diluted in 0.6 ml OptiMEM (Thermo Fisher Scientific): 4.5 µg lentiviral vector, 6 µg psPAX2, and 1.5 µg pMD2.G. Separately, 35 µl of 1 µg/µl 25-kD polyethylenimine (Sigma-Aldrich) was diluted into 0.6 ml OptiMEM and incubated at room temperature for 5 min. After incubation, the DNA and polyethylenimine mixtures were combined, and incubated at room temperature for 20 min. During this incubation, the culture media was replaced with 8 ml pre-warmed DMEM + 1% FBS. The transfection mixture was then added dropwise to the 10 cm dish. Viral particles were harvested 48 h after the media change and filtered through a 0.45 µm PVDF syringe filter. The filtered supernatant was used directly to infect cells. Aliquots were snap-frozen and stored at -80°C. For transduction, lentiviral particles were diluted in complete growth media supplemented with 10 µg/ml polybrene (Sigma-Aldrich) and added to cells.

Gene targeting and generation of stable cell lines

To create RPE1 PLK4^{Dox} and SAS6^{Dox} cells, puromycin-sensitive RPE-1 cells stably expressing Cas9 (Lambrus *et al*, 2016) were transduced with a Tet-ON mPLK4 rTA-IRES-GFP-T2A-Neo or Tet-ON hSAS6 rTA-IRES-GFP-T2A-Neo lentivirus and selected with 400 µg/ml G418 (P212121 cat # LGB-418-10) for 2 weeks. A monoclonal cell

line stably expressing Cas9 and the Tet-ON mPLK4 or Tet-ON hSAS6 transgene was isolated and used in all further experiments.

ANKRD26 rescue cell lines were generated by transducing monoclonal RPE-1 PLK4^{Dox} ANKRD26^{-/-} cells with a CMV-mCherry-ANKRD26-SV40-Zeo lentivirus. Cells were selected in 400 µg/ml zeocin (Invitrogen) for 10 days. PIDD1 rescue cell lines were generated by transducing monoclonal RPE-1 PLK4^{Dox} PIDD1^{-/-} cells with a CMV-PIDD1-SV40-Zeo lentivirus. Cells were selected in 400 µg/ml zeocin (Invitrogen) for 10 days.

To create the DLD1; PIDD1-2xmNeonGreen cell line, an sgRNA targeting the PIDD1 gene (5'-cccagagcctgccagcct-3') was cloned into a pX459 vector (#62988; Addgene). To generate the PIDD1 repair vector, we cloned a 2× mNeonGreen tag followed by a T2A-neomycin and a translational stop codon into a modified pUC vector. 500 bp 5' and 500 bp 3' homology arms were PCR amplified from genomic DLD1 DNA and cloned on either side of the central 2' mNeonGreen-T2A-Neomycin cassette. DLD1 cells were transiently transfected (X-tremeGENE HP, Roche) with the pX459 plasmid and repair vector. Selection of transfected cells was performed 5 days after transfection with 400 µg/ml G418.

Generation of knockout cell lines

RPE-1 PLK4^{Dox} or SAS6^{Dox} cells were transduced with a pLenti-Guide-Puromycin lentivirus containing an sgRNA targeting the gene of interest. Cells were then selected in 1 µg/ml puromycin for 2 days. Knockout cell lines were validated by sequencing genomic DNA to characterize frameshift mutations and loss of signal by either immunoblotting or immunofluorescence. To examine cilia formation, hTERT RPE-1 cells were transduced with a pLentiCRISPR-v2-Neomycin lentivirus containing an sgRNA targeting ANKRD26. Cells were then selected with 400 µg/ml Neo for 7 days.

TIDE

TIDE (Tracking of Indels by Decomposition) was used to estimate the INDEL efficiency in the polyclonal Plk4^{Dox} knockout cells shown in Fig 1G and H (Brinkman *et al*, 2014). To calculate the frequency of frameshift mutations, INDELs in the +3, +6, +9, -3, -6, -9 reading frames were excluded from the final calculation.

Growth assays

For competition growth assays, RPE-1 PLK4^{Dox} cells constitutively expressing EGFP and non-fluorescent RPE1 cells were mixed at a 1:1 ratio and seeded into duplicate wells. One well from each pair was treated with doxycycline. After 5 days, each well was trypsinized and analyzed on a Guava easyCyte flow cytometer to determine the fraction of GFP-positive cells. For each well, the fraction of GFP-positive cells was divided by the GFP-negative cells. The value obtained from the doxycycline treated well was then divided by that obtained in the untreated well to determine the fold change in GFP-positive cells.

For long-term growth assays, RPE-1 PLK4^{Dox} cells were seeded into duplicate wells and one well from each pair was treated with 1 µg/ml doxycycline. Cell number was counted every 2 days in triplicate using a LUNA-II automated cell counter.

Co-immunoprecipitation

Co-immunoprecipitation was performed as previously described (Moyer *et al*, 2015). 2×10^6 HEK293FT cells were seeded into 10 cm² dishes and 24 h later were transfected with plasmid DNA. 48 h later, transfected cells were lysed in lysis buffer [10 mM Tris pH 7.5, 0.1% Triton X-100, 250 mM NaCl, 1 mM EDTA, 50 mM NaF, 50 mM β-glycerophosphate, 1 mM DTT, 500 nM microcystin, 1 mM PMSF and EDTA-free protease inhibitor tablet (Roche)], sonicated and soluble extracts prepared. The supernatant was incubated with beads coupled to either GFP-binding or mCherry-binding protein (Rothbauer *et al*, 2008). Beads were washed three times in lysis buffer, and immunopurified protein was analyzed by immunoblot.

Immunoblotting and immunofluorescence

Immunoblotting and immunofluorescence were performed as previously described (Moyer *et al*, 2015). For immunoblot analysis, protein samples were separated by SDS-PAGE, transferred onto nitrocellulose membranes with a Trans-Blot Turbo Transfer System (BioRad) or by overnight wet-transfer and probed with the following antibodies: alpha-tubulin (rat, Y1/2, Invitrogen, MA180017, 1:1,000), ANKRD26 (rabbit, GeneTex, GTX128255, 1:1,000), PIDD1 (mouse, Enzo, ALX-804837C100, 1:500), caspase 2 (rat, 11B4, Millipore Sigma, MAB3507, 1:1,000), TRIM37 (rabbit, Bethyl Laboratories, A301-174A-M, 1:1,000), and p21^{WAF1} (mouse, Ab-1, Cal Biochem, OP64, 1:100). Blots were blocked with 5% milk in TBST and washed with TBST.

For immunofluorescence, cells were grown on 18-mm glass coverslips and fixed in 100% -20°C methanol for 10 min. Cells were blocked in 2.5% FBS, 200 mM glycine, and 0.1% Triton X-100 in PBS for 1 h. Antibody incubations were conducted in the blocking solution for 1 h. DNA was detected using DAPI, and cells were mounted in Prolong Antifade (Invitrogen). Staining was performed with the following primary antibodies: USP28 (rabbit, Proteintech, 17707-1-AP, 1:1,000), Centrin (rabbit, directly conjugated, (Moyer & Holland, 2019), 1:1,000), CEP192 (goat, directly labeled, (Moyer & Holland, 2019), 1:1,000), SCLT1 (rat, (Tanos *et al*, 2013), 1:250), CEP83 (rabbit, Sigma-Aldrich, HPA038161, 1:200), CEP89 (rat, (Tanos *et al*, 2013), 1:500), 1:1,000), Polyglutamylolation (mouse, GT335, AdipoGen, AG-20B-0020-C100), FOPNL/FOR20 (rat, (Sedjāi *et al*, 2010), 1:500), C2CD3 (rabbit, Atlas Antibodies, HPA038552, 1:500), and CEP164 (rabbit, Millipore Sigma, AEB2621, 1:1,000). Secondary donkey antibodies were conjugated to Alexa Fluor[®] 488, 555, or 650 (Life Technologies).

Immunofluorescence images were collected using a Deltavision Elite system (GE Healthcare) controlling a Scientific CMOS camera (pco.edge 5.5). Acquisition parameters were controlled by SoftWoRx suite (GE Healthcare). Images were collected at room temperature using an Olympus 60× 1.42 NA or Olympus 100× 1.4 NA oil objective at 0.2 µm z-sections and subsequently deconvolved in SoftWoRx suite. Images were acquired using Applied Precision immersion oil ($N = 1.516$).

Cilia assembly

hTERT RPE-1 cells were grown to confluency on 18-mm glass coverslips and then placed in serum-free media (DMEM:F12 50:50

medium supplemented with 0.348% sodium bicarbonate, 100 U/ml penicillin, 100 U/ml streptomycin, and 2 mM L-glutamine) for 2 days. Prior to fixation, cells were washed with 1× PBS and incubated in microtubule stabilization buffer (30% glycerol, 100 mM PIPES, 1 mM EGTA, 1 mM MgSO₄) for 30 s. Cells were then washed with PBS and processed for immunofluorescence staining.

Cytokinesis failure assay

To look at the effects of cytokinesis failure, PLK4^{Dox} cells were seeded in duplicate wells. One well was treated with 10 µg/ml cytochalasin B (Sigma-Aldrich), and the other well was treated with DMSO for 24 h. Cells were then washed with media 3 times, and then, fresh media were added to cells supplemented with 10 µM EdU (Invitrogen) and 10 µM Dimethylnastron (DMN) (Sigma-Aldrich). Cells were incubated for 24 h. Cells were then collected and fixed with 100% ethanol at −20°C for at least 1 h. Each sample was washed with PBS then stained with a Click-iT reaction for 30 min in the dark. The Click-iT reaction was prepared following manufacturer's protocol (Invitrogen). Samples were washed and stained with a 25 µg/ml propidium iodide solution supplemented with RNase A (Sigma-Aldrich) for 30 min in the dark. Samples were analyzed on a BD FACSCalibur flow cytometer to determine DNA content and EdU incorporation. The percent of EdU-positive cells with a DNA content of greater than 4N was determined for each sample. The DMSO-treated sample was subtracted from the cytochalasin B-treated sample for each cell line.

Griseofulvin assay

Cells were grown on 18-mm glass coverslips and treated with griseofulvin for 24 h. Cells were then fixed in 100% −20°C methanol for 10 min and processed for immunofluorescence staining. Anaphase cells were imaged, and spindle morphology scored.

EdU incorporation

PLK4^{Dox} cells were seeded in duplicate wells and one was treated with one of the following drugs: doxorubicin for 2 days, reversine for 2 days, centrinone for 5 days or H₂O₂ for 2 h followed by an overnight incubation in fresh media. Both the treated and untreated wells were seeded onto 18-mm glass coverslips and incubated in media supplemented with 10 µM EdU for 24 h. Cells were then fixed in 100% −20°C methanol for 10 min, washed with PBST and stained with a Click-iT reaction for 30 min in the dark to label EdU. Each coverslip was incubated with 197.2 µl 1× PBS, 2.5 µl 100 mM CuSO₄, 50 µl 500 mM Ascorbic Acid (prepared fresh), and 0.3 µl 125 µM Azide-fluor 488 (Millipore Sigma). After 30 min, cells were rinsed with PBS, DAPI stained, and then mounted with Prolong Antifade.

Immunofluorescence for STORM

Cells were grown on 25 mm, 1.5 high tolerance coverslips (Warner Instruments). Cells were fixed in 1.5% formaldehyde for 4 min then permeabilized in 0.05% Triton for 30 s. Samples were washed in 1× PBS and blocked in IF buffer (1% BSA, 0.05% Tween-20, in 1× PBS) for 15 min. Cells were incubated with primary antibody diluted in

IF buffer at 37°C for 3 h. After washing in 1× PBS, cells were incubated with secondary antibody diluted IF buffer at 37°C for 3 h. The following primary antibodies were used: CEP164 (rabbit, recognizing aa: 1–112, Proteintech, 22227-1-AP, 1:3,500), PIDD1 (mouse, Enzo, ALX-804837C100, 1:500). Conjugated secondary antibodies CF647 anti-mouse (Biotium, 20042) and CF568 anti-rabbit (Biotium, 20099) were used at 1:800 dilution.

Stochastic optical reconstruction microscopy (STORM)

Samples were layered with 100 nm tetra-spectral fluorescent spheres (Invitrogen), which served as fiducial markers. Coverslips were mounted in Attofluor Cell chambers (Thermo Fisher) in imaging buffer (25 mM β-mercaptoethylamine, 0.5 mg/ml glucose oxidase, 67 µg/ml catalase, 10% dextrose, in 100 mM Tris at pH 8.0). 3D STORM imaging was performed on a Nikon N-STORM4.0 system using an Eclipse Ti inverted microscope, Apo TIRF 100× SA NA 1.49 Plan Apo oil objective, 405, 561, 488, and 647 nm excitation laser launch and a back-illuminated EMCCD camera (Andor, DU897). The 647 nm laser line (~150 mW out of the fiber and ~90 mW before the objective lens) was used to promote fluorophore blinking. The 405 nm laser was used to reactivate fluorophores. The 561 nm laser was used to record the signals of fiducial markers. 20,000 to 30,000-time points were acquired at a 50 Hz frame rate each 16–20 ms. NIS Elements (Nikon) were used to analyze the data.

Prior to STORM imaging, the position of CEP164 and PIDD1 was recorded in wide-field mode. The original storm Z color coding scheme illustrating the calibrated Z range (from red for the signals closer to the coverslip to blue for the signals further from the coverslip) is preserved on STORM images, which are presented as a projection of the entire 3D volume. The outer and inner diameters of distal appendage proteins were determined by measuring the diameters of the circles outlining the outer and inner edges of the STORM signal (Bowler *et al*, 2019).

CRISPR/Cas9 genome-wide screen

CRISPR/Cas9 pooled, knockout screens were performed essentially as described (Shalem *et al*, 2014; Chen *et al*, 2015; Lambrus *et al*, 2016). RPE-1 PLK4^{Dox} cells were infected with a lentivirus containing an sgRNA targeting TRIM37 or USP28. The sgRNA sequence targeting TRIM37 was CTCTAATTTAAATAGCATGG. The sgRNA sequence targeting USP28 was ATCAACTCTCTCCAGTCAT. Infected cells were then selected with 400 µg/ml zeocin for 3 weeks and monoclonal knockout lines isolated and validated by immunoblotting.

The human Brunello CRISPR knockout sgRNA library was purchased from Addgene (a gift of David Root and John Doench; #73178) and plasmid DNA amplified according to the manufacturer's instructions. To produce virus, the Brunello pooled plasmid library and the lentiviral packaging plasmids psPAX2 and pMD2.G were co-transfected into 40 × 15 cm culture dishes of HEK293FT cells. 6 × 10⁶ HEK293FT cells were seeded into a poly-L-Lysine-coated 15 cm culture dish the day before transfection. For each 15 cm dish, the following DNA was diluted in 1.2 ml OptiMEM (Thermo Fisher Scientific): 9 µg lentiviral vector, 12 µg psPAX2, and 3 µg pMD2.G. Separately, 70 µl of 1 µg/µl 25-kD

polyethylenimine (Sigma-Aldrich) was diluted into 1.2 ml OptiMEM and incubated at room temperature for 5 min. After incubation, the DNA and polyethylenimine mixtures were combined and incubated at room temperature for 20 min. During this incubation, the culture media were replaced with 16 ml prewarmed DMEM + 1% FBS. The transfection mixture was then added dropwise to the 15 cm dish. Viral particles were harvested at 24, 48, and 72 h after the media change. Media collected from 24, 48, and 72 h was pooled and filtered through a 0.45 μ m PVDF syringe filter. The media were then concentrated using Amicon Ultra-15 Centrifugal Filter Unit with Ultracel-50 membrane (EMD Millipore Corporation cat# UFC905024). The virus was then frozen and stored at -80°C .

Cells were transduced with the Brunello library via spinfection as previously described (Lambrus *et al*, 2016). To find the optimal virus volumes for achieving an MOI ~ 0.1 , each new batch of virus was titered by spinfecting 3×10^6 cells with several different volumes of virus. Briefly, 3×10^6 cells per well were seeded into a 12 well plate in growth media supplemented with 10 $\mu\text{g/ml}$ polybrene. Each well received a different titrated virus amount (between 5 and 50 μl) along with a no-transduction control. The plate was centrifuged at 872 g for 2 h at room temperature. After the spin, media were aspirated, and fresh growth media were added. The following day, cells were counted, and each well was split into duplicate wells. One well received 3 $\mu\text{g/ml}$ puromycin (Sigma) for 3 days. Cells were counted and the percent transduction calculated as the cell count from the replicate with puromycin divided by the cell count from the replicate without puromycin multiplied by 100. The virus volume yielding a MOI closest to 0.1 was chosen for large-scale transductions.

For the pooled screen, a total of 1×10^8 PLK4^{Dox}; TRIM37^{-/-}; or PLK4^{Dox}; USP28^{-/-} cells were infected at MOI ~ 0.1 and selected with puromycin at 3 $\mu\text{g/ml}$ for 3 days. MOI was calculated using a control well infected in parallel following the same procedure outlined above. Infected cells were expanded under puromycin selection for 5 days and then seeded into 80 \times 15 cm dishes with 250,000 cells per dish. 40 of the dishes received media supplemented with 400 $\mu\text{g/ml}$ of G418 to maintain selection for the Tet-ON mPLK4 transgene and the other 40 dishes received 1 $\mu\text{g/ml}$ of doxycycline and 400 $\mu\text{g/ml}$ of G418. Cells were allowed to grow for 21 days without further passaging before being harvested for DNA extraction.

Cell pellets were resuspended in lysis buffer containing 50 mM Tris, 50 mM EDTA, 1% SDS, pH 8, and 30 μl of 20 mg/ml proteinase K and incubated at 55°C overnight. The next day, 30 μl of 10 mg/ml RNase A was added, and the sample was inverted 25 times and incubated at 37°C for 30 min. Samples were cooled on ice before adding 2 ml of chilled 7.5 M ammonium acetate. Samples were then vortexed at high speed for 20 s and centrifuged at $> 4,000$ g for 10 min. The supernatants were decanted into new 15 ml conical tubes, and 6 ml of 100% isopropanol was added. The tubes were inverted 50 times and centrifuged at $> 4,000$ g for 10 min. The supernatant was discarded, and 6 ml of freshly prepared 70% ethanol was added to each tube. The tubes were inverted 10 times and centrifuged at $> 4,000$ g for 1 min. The supernatant was discarded, and the pellet was air dried for 30 min. Finally, 200 μl of $1 \times$ TE buffer was added, and the tube was

incubated at 65°C for 1 h. DNA concentration was measured using a Nanodrop.

The sgRNA library for each sample was amplified and prepared for Illumina sequencing using a two-step PCR procedure as previously described (Lambrus *et al*, 2016). For the first PCR, a region containing the sgRNA cassette was amplified using primers specific to the sgRNA-expression vector:

lentiGuide-PCR-F: AATGGACTATCATATGCTTACCGTAACTGAAAGTATTTCC

lentiGuide-PCR1-R: CTTTAGTTTGTATGTCTGTTGCTATTATGTCTACTATTCTTTCC

The thermocycling parameters for the first PCR were as follows: 98°C for 30 s, 18–24 cycles of (98°C for 1 s, 62°C for 5 s, 72°C for 35 s), and 72°C for 1 min. 1.5 μg of DNA was used in each PCR reaction. Assuming 6.6 pg of DNA per cell, $\sim 100\times$ representation of the Brunello library required ~ 53 μg of DNA per sample (36 PCR reactions). The resulting amplicons for each sample were pooled, gel purified, and used for amplification with barcoded second PCR primers. For each sample, we performed 12 reactions.

Primers for the second PCR include both a variable length sequence to increase library complexity and an 8 bp barcode for multiplexing of different biological samples:

F2: AATGATACGGCGACCACCGAGATCTACACTCTTTCCCTACACGACGCTCTTCCGATCT(4–7 bp random nucleotides) (8 bp barcode) TCTTGTGGAAAGGACGAAACACCG

R2: CAAGCAGAAGACGGCATAACGAGATGTGACTGGAGTTCAGACGTGTGCTCTTCCGATCTTCTACTATTCTTTCCCTGCAGTGT

5 μl of the product from the first PCR reaction was used, and the thermocycling parameters for the second PCR were as follows: 98°C for 30 s, 18–24 cycles of (98°C for 1 s, 70°C for 5 s, 72°C for 35 s). Second PCR products were pooled, gel purified, and quantified using the Next Library Quantification Kit (NEB). Diluted libraries with 5% PhiX were sequenced with MiSeq (Illumina).

Sequencing data were processed for sgRNA representation using custom scripts. Briefly, sequencing reads were first demultiplexed using the barcodes in the forward primer and then trimmed to leave only the 20 bp sgRNA sequences. The spacer sequences were then mapped to the spacers of the designed sgRNA library using Bowtie (Langmead *et al*, 2009). For mapping, a maximum of one mismatch was allowed in the 20 bp sgRNA sequence. Mapped sgRNA sequences were then quantified by counting the total number of reads. The total numbers of reads for all sgRNAs in each sample were normalized.

The screen was performed two independent times for both PLK4^{Dox}, TRIM37^{-/-}, and PLK4^{Dox}, USP28^{-/-} cells. We used the MaGeCK scoring algorithm (model-based analysis of genome-wide CRISPR-Cas9 knockout) to analyze and the rank the genes from the screens (Li *et al*, 2014). We noted that some of the hits from the MaGeCK analysis contained sgRNAs with very low representation (Cerami *et al*, 2012). Among these low count, hits were many mitochondria and ATP production related genes that are likely selected for by the doxycycline treatment. We therefore excluded all genes that did not show a $\geq 0.005\%$ representation for at least two sgRNAs from the doxycycline-treated population from any transduction of either the

PLK4^{Dox}; TRIM37^{-/-} or PLK4^{Dox}; USP28^{-/-} cell lines. Genes with an FDR cutoff of ≤ 0.4 were taken forward for further validation.

ANKRD26 cancer mutation

The ANKRD26 K1234Nfs*19 cancer mutation was identified from the curated set of non-redundant studies in cBioportal (<https://www.cbioportal.org>) (Cerami et al, 2012).

Quantification and statistical analysis

Statistical analysis was performed using GraphPad Prism software. Differences between samples were tested using a two-tailed Student's *t*-test and annotated following the nomenclature: ns ($P > 0.05$), * ($P \leq 0.05$), ** ($P \leq 0.01$), *** ($P \leq 0.001$), and **** ($P \leq 0.0001$).

Data availability

This study includes no data deposited in external repositories.

Expanded View for this article is available online.

Acknowledgements

This work was supported by the National Institutes of Health grants R01GM114119 and R01GM133897, an American Cancer Society Scholar grant RSG-16-156-01-CCG, and an American Cancer Society Mission Boost Grant MBG-19-173-01-MBG (to A.J.H.). L.T. Evans was funded by National Institutes of Health training grant (T32GM007814) and a National Science Foundation Graduate Research Fellowship. J.L. was supported by the Intramural Research Program of the National Institutes of Health (NIH), National Cancer Institute, Center for Cancer Research.

Author contributions

AJH and LTE conceived the project. LTE performed and analyzed the majority of the experiments and prepared the figures. TA performed the genome-wide CRISPR screen. PS performed the co-immunoprecipitation experiments. KL and JL performed the STORM imaging of PIDD1. AJH and LTE wrote the manuscript. All authors edited the manuscript. AJH conceived and supervised the study.

Conflict of interest

The authors that they have no conflict of interest.

References

- Alves-Cruzeiro JM, Nogales-Cadenas R, Pascual-Montano AD (2014) CentrosomeDB: a new generation of the centrosomal proteins database for human and *Drosophila melanogaster*. *Nucleic Acids Res* 42: D430–D436
- Annandis T, Monteiro P, Adams SD, Bridgeman VL, Rajeev V, Gadaleta E, Marzec J, Chelala C, Malanchi I, Cutillas PR et al (2018) Oxidative stress in cells with extra centrosomes drives non-cell-autonomous invasion. *Dev Cell* 47: 409–424
- Arquint C, Gabryjonczyk AM, Nigg EA (2014) Centrosomes as signalling centres. *Philos Trans R Soc Lond B Biol Sci* 369: 20130464
- Basto R, Brunk K, Vinadogrova T, Peel N, Franz A, Khodjakov A, Raff JW (2008) Centrosome amplification can initiate tumorigenesis in flies. *Cell* 133: 1032–1042
- Bielski CM, Zehir A, Penson AV, Donoghue MTA, Chatila W, Armenia J, Chang MT, Schram AM, Jonsson P, Bandlamudi C et al (2018) Genome doubling shapes the evolution and prognosis of advanced cancers. *Nat Genet* 50: 1189–1195
- Bluteau D, Balduini A, Balayn N, Currao M, Nurden P, Deswarte C, Leverger G, Noris P, Perrotta S, Solary E et al (2014) Thrombocytopenia-associated mutations in the ANKRD26 regulatory region induce MAPK hyperactivation. *J Clin Invest* 124: 580–591
- Bowler M, Kong D, Sun S, Nanjundappa R, Evans L, Farmer V, Holland A, Mahjoub MR, Sui H, Loncarek J (2019) High-resolution characterization of centriole distal appendage morphology and dynamics by correlative STORM and electron microscopy. *Nat Commun* 10: 993
- Brinkman EK, Chen T, Amendola M, van Steensel B (2014) Easy quantitative assessment of genome editing by sequence trace decomposition. *Nucleic Acids Res* 42: e168
- Cerami E, Gao J, Dogrusoz U, Gross BE, Sumer SO, Aksoy BA, Jacobsen A, Byrne CJ, Heuer ML, Larsson E et al (2012) The cBio cancer genomics portal: an open platform for exploring multidimensional cancer genomics data. *Cancer Discov* 2: 401–404
- Chan JY (2011) A clinical overview of centrosome amplification in human cancers. *Int J Biol Sci* 7: 1122–1144
- Chen S, Sanjana NE, Zheng K, Shalem O, Lee K, Shi X, Scott DA, Song J, Pan JQ, Weissleder R et al (2015) Genome-wide CRISPR screen in a mouse model of tumor growth and metastasis. *Cell* 160: 1246–1260
- Coelho PA, Bury L, Shahbazi MN, Liakath-Ali K, Tate PH, Wormald S, Hindley CJ, Huch M, Archer J, Skarnes WC et al (2015) Over-expression of Plk4 induces centrosome amplification, loss of primary cilia and associated tissue hyperplasia in the mouse. *Open Biol* 5: 150209
- Crasta K, Ganem NJ, Dagher R, Lantermann AB, Ivanova EV, Pan Y, Nezi L, Protopopov A, Chowdhury D, Pellman D (2012) DNA breaks and chromosome pulverization from errors in mitosis. *Nature* 482: 53–58
- Falcieri E, Bassini A, Pierpaoli S, Luchetti F, Zamai L, Vitale M, Guidotti L, Zauli G (2000) Ultrastructural characterization of maturation, platelet release, and senescence of human cultured megakaryocytes. *Anat Rec* 258: 90–99
- Fava LL, Schuler F, Sladky V, Haschka MD, Soratroi C, Eiterer L, Demetz E, Weiss G, Geley S, Nigg EA et al (2017) The PIDDosome activates p53 in response to supernumerary centrosomes. *Genes Dev* 31: 34–45
- Firat-Karalar EN, Stearns T (2014) The centriole duplication cycle. *Philos Trans R Soc Lond B Biol Sci* 369: 20130460
- Fong CS, Mazo G, Das T, Goodman J, Kim M, O'Rourke BP, Izquierdo D, Tsou MF (2016) 53BP1 and USP28 mediate p53-dependent cell cycle arrest in response to centrosome loss and prolonged mitosis. *Elife* 5: e16270
- Fu J, Hagan IM, Glover DM (2015) The centrosome and its duplication cycle. *Cold Spring Harb Perspect Biol* 7: a015800
- Ganem NJ, Godinho SA, Pellman D (2009) A mechanism linking extra centrosomes to chromosomal instability. *Nature* 460: 278–282
- Ganem NJ, Pellman D (2012) Linking abnormal mitosis to the acquisition of DNA damage. *J Cell Biol* 199: 871–881
- Ganem NJ, Cornils H, Chiu SY, O'Rourke KP, Arnaud J, Yimlamai D, Thery M, Camargo FD, Pellman D (2014) Cytokinesis failure triggers hippo tumor suppressor pathway activation. *Cell* 158: 833–848

- Ganier O, Schnerch D, Nigg EA (2018a) Structural centrosome aberrations sensitize polarized epithelia to basal cell extrusion. *Open Biol* 8: 180044
- Ganier O, Schnerch D, Oertle P, Lim RY, Plodinec M, Nigg EA (2018b) Structural centrosome aberrations promote non-cell-autonomous invasiveness. *EMBO J* 37: e98576
- Godinho SA, Picone R, Burute M, Dagher R, Su Y, Leung CT, Polyak K, Brugge JS, They M, Pellman D (2014) Oncogene-like induction of cellular invasion from centrosome amplification. *Nature* 510: 167–171
- Gonczy P (2012) Towards a molecular architecture of centriole assembly. *Nat Rev Mol Cell Biol* 13: 425–435
- Hagan IM, Grallert A (2013) Spatial control of mitotic commitment in fission yeast. *Biochem Soc Trans* 41: 1766–1771
- Holland AJ, Fachinetti D, Zhu Q, Bauer M, Verma IM, Nigg EA, Cleveland DW (2012) The autoregulated instability of Polo-like kinase 4 limits centrosome duplication to once per cell cycle. *Genes Dev* 26: 2684–2689
- Janssen A, van der Burg M, Suzhai K, Kops GJ, Medema RH (2011) Chromosome segregation errors as a cause of DNA damage and structural chromosome aberrations. *Science* 333: 1895–1898
- Lambrus BG, Daggubati V, Uetake Y, Scott PM, Clutario KM, Sluder G, Holland AJ (2016) A USP28-53BP1-p53-p21 signaling axis arrests growth after centrosome loss or prolonged mitosis. *J Cell Biol* 214: 143–153
- Langmead B, Trapnell C, Pop M, Salzberg SL (2009) Ultrafast and memory-efficient alignment of short DNA sequences to the human genome. *Genome Biol* 10: R25
- Levine MS, Bakker B, Boeckx B, Moyett J, Lu J, Vitre B, Spierings DC, Lansdorp PM, Cleveland DW, Lambrechts D et al (2017) Centrosome amplification is sufficient to promote spontaneous tumorigenesis in mammals. *Dev Cell* 40: 313–322
- Li W, Xu H, Xiao T, Cong L, Love MI, Zhang F, Irizarry RA, Liu JS, Brown M, Liu XS (2014) MAGeCK enables robust identification of essential genes from genome-scale CRISPR/Cas9 knockout screens. *Genome Biol* 15: 554
- LoMastro GM, Holland AJ (2019) The emerging link between centrosome aberrations and metastasis. *Dev Cell* 49: 325–331
- Marconi C, Canobbio I, Bozzi V, Pippucci T, Simonetti G, Melazzini F, Angori S, Martinelli G, Saglio G, Torti M et al (2017) 5'UTR point substitutions and N-terminal truncating mutations of ANKRD26 in acute myeloid leukemia. *J Hematol Oncol* 10: 18
- Marquez R, Hantel A, Lorenz R, Neistadt B, Wong J, Churpek JE, Mardini NA, Shaukat I, Gurbuxani S, Miller JL et al (2014) A new family with a germline ANKRD26 mutation and predisposition to myeloid malignancies. *Leuk Lymphoma* 55: 2945–2946
- Meitinger F, Anzola JV, Kaulich M, Richardson A, Stender JD, Benner C, Glass CK, Dowdy SF, Desai A, Shiau AK et al (2016) 53BP1 and USP28 mediate p53 activation and G1 arrest after centrosome loss or extended mitotic duration. *J Cell Biol* 214: 155–166
- Moskvin-Tarkhanov MI, Onishchenko GE (1978) Centrioles in mouse bone marrow megakaryocytes. *Tsitologiya* 20: 1436–1438
- Moyer TC, Clutario KM, Lambrus BG, Daggubati V, Holland AJ (2015) Binding of STIL to Plk4 activates kinase activity to promote centriole assembly. *J Cell Biol* 209: 863–878
- Moyer TC, Holland AJ (2019) PLK4 promotes centriole duplication by phosphorylating STIL to link the procentriole cartwheel to the microtubule wall. *Elife* 8: e46054
- Nigg EA, Stearns T (2011) The centrosome cycle: centriole biogenesis, duplication and inherent asymmetries. *Nat Cell Biol* 13: 1154–1160
- Nigg EA, Holland AJ (2018) Once and only once: mechanisms of centriole duplication and their deregulation in disease. *Nat Rev Mol Cell Biol* 19: 297–312
- Noris P, Favier R, Alessi MC, Geddis AE, Kunishima S, Heller PG, Giordano P, Niederhoffer KY, Bussel JB, Podda GM et al (2013) ANKRD26-related thrombocytopenia and myeloid malignancies. *Blood* 122: 1987–1989
- Oliver TG, Meylan E, Chang GP, Xue W, Burke JR, Humpton TJ, Hubbard D, Bhutkar A, Jacks T (2011) Caspase-2-mediated cleavage of Mdm2 creates a p53-induced positive feedback loop. *Mol Cell* 43: 57–71
- Park HH, Logette E, Raunser S, Cuenin S, Walz T, Tschopp J, Wu H (2007) Death domain assembly mechanism revealed by crystal structure of the oligomeric PIDDosome core complex. *Cell* 128: 533–546
- Pippucci T, Savoia A, Perrotta S, Pujol-Moix N, Noris P, Castegnaro G, Pecci A, Gnan C, Punzo F, Marconi C et al (2011) Mutations in the 5' UTR of ANKRD26, the ankirin repeat domain 26 gene, cause an autosomal-dominant form of inherited thrombocytopenia, THC2. *Am J Hum Genet* 88: 115–120
- Rebacz B, Larsen TO, Clausen MH, Ronnest MH, Loffler H, Ho AD, Kramer A (2007) Identification of griseofulvin as an inhibitor of centrosomal clustering in a phenotype-based screen. *Cancer Res* 67: 6342–6350
- Rothbauer U, Zolghadr K, Muyldermans S, Schepers A, Cardoso MC, Leonhardt H (2008) A versatile nanotrapp for biochemical and functional studies with fluorescent fusion proteins. *Mol Cell Proteomics* 7: 282–289
- Sedjai F, Acquaviva C, Chevrier V, Chauvin JP, Coppin E, Auouane A, Coulier F, Tolun A, Pierres M, Birnbaum D et al (2010) Control of ciliogenesis by FOR20, a novel centrosome and pericentriolar satellite protein. *J Cell Sci* 123(Pt 14): 2391–2401
- Sercin O, Larsimont JC, Karambelas AE, Marthiens V, Moers V, Boeckx B, Le Mercier M, Lambrechts D, Basto R, Blanpain C (2016) Transient PLK4 overexpression accelerates tumorigenesis in p53-deficient epidermis. *Nat Cell Biol* 18: 100–110
- Shalem O, Sanjana NE, Hartenian E, Shi X, Scott DA, Mikkelsen TS, Heckl D, Ebert BL, Root DE, Doench JG et al (2014) Genome-scale CRISPR-Cas9 knockout screening in human cells. *Science* 343: 84–87
- Silkworth WT, Nardi IK, Scholl LM, Cimini D (2009) Multipolar spindle pole coalescence is a major source of kinetochore mis-attachment and chromosome mis-segregation in cancer cells. *PLoS One* 4: e6564
- Sladky V, Schuler F, Fava LL, Villunger A (2017) The resurrection of the PIDDosome – emerging roles in the DNA-damage response and centrosome surveillance. *J Cell Sci* 130: 3779–3787
- Sladky VC, Knapp K, Soratroi C, Heppke J, Eichin F, Rocamora-Reverte L, Szabo TG, Bongiovanni L, Westendorp B, Moreno E et al (2020) E2F-family members engage the PIDDosome to limit hepatocyte ploidy in liver development and regeneration. *Dev Cell* 52: 335–349
- Sladky VC, Villunger A (2020) Uncovering the PIDDosome and caspase-2 as regulators of organogenesis and cellular differentiation. *Cell Death Differ* 27: 2037–2047
- Tanos BE, Yang HJ, Soni R, Wang WJ, Macaluso FP, Asara JM, Tsou MF (2013) Centriole distal appendages promote membrane docking, leading to cilia initiation. *Genes Dev* 27: 163–168
- Tinel A, Tschopp J (2004) The PIDDosome, a protein complex implicated in activation of caspase-2 in response to genotoxic stress. *Science* 304: 843–846
- Tinel A, Janssens S, Lippens S, Cuenin S, Logette E, Jaccard B, Quadroni M, Tschopp J (2007) Autoproteolysis of PIDD marks the bifurcation between pro-death caspase-2 and pro-survival NF- κ B pathway. *EMBO J* 26: 197–208

- Tsou MF, Stearns T (2006) Controlling centrosome number: licenses and blocks. *Curr Opin Cell Biol* 18: 74–78
- Vitrat N, Cohen-Solal K, Pique C, Le Couedic JP, Norol F, Larsen AK, Katz A, Vainchenker W, Debili N (1998) Endomitosis of human megakaryocytes are due to abortive mitosis. *Blood* 91: 3711–3723
- Wang R, Wei Z, Jin H, Wu H, Yu C, Wen W, Chan LN, Wen Z, Zhang M (2009) Autoinhibition of UNC5b revealed by the cytoplasmic domain structure of the receptor. *Mol Cell* 33: 692–703
- Wang M, Nagle RB, Knudsen BS, Cress AE, Rogers GC (2019) Centrosome loss results in an unstable genome and malignant prostate tumors. *Oncogene* 39: 399–413
- Yang TT, Chong WM, Wang WJ, Mazo G, Tanos B, Chen Z, Tran TMN, Chen YD, Weng RR, Huang CE et al (2018) Super-resolution architecture of mammalian centriole distal appendages reveals distinct blade and matrix functional components. *Nat Commun* 9: 2023
- Ye X, Zeng H, Ning G, Reiter JF, Liu A (2014) C2cd3 is critical for centriolar distal appendage assembly and ciliary vesicle docking in mammals. *Proc Natl Acad Sci USA* 111: 2164–2169
- Zack TI, Schumacher SE, Carter SL, Cherniack AD, Saksena G, Tabak B, Lawrence MS, Zhsng CZ, Wala J, Mermel CH et al (2013) Pan-cancer patterns of somatic copy number alteration. *Nat Genet* 45: 1134–1140